Remote Sensing of Environment 120 (2012) 164–174

Contents lists available at SciVerse ScienceDirect

Remote Sensing of Environment

journal homepage: www.elsevier.com/locate/rse

The Sentinel-1 mission for the improvement of the scientific understanding and the operational monitoring of the seismic cycle

S. Salvi [a,*], S. Stramondo [a], G.J. Funning [b], A. Ferretti [c], F. Sarti [d], A. Mouratidis [d]

[a] Istituto Nazionale di Geofisica e Vulcanologia, Via di Vigna Murata, 605, 00142 Roma, Italy
[b] University of California, 900 University Ave., Riverside, CA 92521, USA
[c] TeleRilevamento Europa, Via Vittoria Colonna, 7, 20149 Milano,Italy
[d] European Space Agency, ESA/ESRIN, V.Galileo Galilei, C.P. 64, 00044 Frascati, Italy

ARTICLE INFO

Article history:
Received 7 January 2011
Received in revised form 6 August 2011
Accepted 10 September 2011
Available online 14 March 2012

Keywords:
SAR Interferometry
Seismic cycle
Seismic hazard
Satellite Earth observation

ABSTRACT

We describe the state of the art of scientific research on the earthquake cycle based on the analysis of Synthetic Aperture Radar (SAR) data acquired from satellite platforms. We examine the achievements and the main limitations of present SAR systems for the measurement and analysis of crustal deformation, and envision the foreseeable advances that the Sentinel-1 data will generate in the fields of geophysics and tectonics. We also review the technological and scientific issues which have limited so far the operational use of satellite data in seismic hazard assessment and crisis management, and show the improvements expected from Sentinel-1 data.

1. Introduction

Earthquakes and fault ruptures cannot be directly observed at the depths at which they originate. This, and the fact that earthquake processes span several orders of magnitude of space and time scales, complicates the scientific understanding of these phenomena (Rundle et al., 2003). Seismology is in fact a science largely based on observations not only of present events, but also of those registered in the historical and geological records. During the last couple of decades, our understanding of earthquake and fault processes has improved, thanks to new observational methods, as broadband seismology, Global Positioning System (GPS) and SAR Interferometry (InSAR).

Development of new observation tools and datasets has always led in short order to scientific advancements. For example, plate tectonics, the most revolutionary Earth science theory of the past century, could only be fully developed when new, improved, and systematic observations of the Earth's gravity and magnetic fields, precise locations of global earthquakes and detailed measurements of seafloor bathymetry, started to become available in the 1950s and 1960s.

Today the Solid Earth scientist has the technological means to generate a wealth of spatially and temporally denser observations to constrain better earthquake models and improve the understanding of the fundamental physical processes driving the earthquake cycle. What is really needed is to make these observations systematic and constant over a long period of time. Measurement instruments placed on satellite platforms are among the best ways to provide systematic observation of the Earth surface over large areas and over long time intervals. In the field of geophysics the most successful of such instruments in the last two decades has been the Synthetic Aperture Radar (SAR).

Using SAR images of the ground acquired at different times, an accurate, quantitative measurement of the deformation of the Earth's crust can be obtained. This is one of the most important parameters for the study of the seismic cycle, providing important constraints that are used to model the mechanisms of tectonic stress accumulation (in the interseismic phase) and release (in the coseismic and postseismic phases) along fault zones.

Since the 1990s two Earth Observation missions of the European Space Agency (ESA) have provided fundamental SAR data for these applications. The ERS and ENVISAT missions were very successful not only in promoting new Earth science applications: based on these data new analysis techniques have been developed, tested, and standardized for use by service providers in the market (Adam et al., 2009; Berardino et al., 2002; Ferretti et al., 2000).

The Sentinel-1 mission has been designed to continue, and improve, the data flow provided by previous ESA SAR missions (see the introductory article in this issue), and to provide the framework for the development of operational services and applications.

The aim of this paper is to describe the advances and potential that the Sentinel-1 data are expected to generate in the fields of seismology and seismic risk management. We shall review the applications of SAR data for the scientific understanding of the seismic cycle and

* Corresponding author. Tel.: +39 06 51860438; fax: +39 06 5041181.
E-mail address: stefano.salvi@ingv.it (S. Salvi).

0034-4257/$ – see front matter © 2012 Elsevier Inc. All rights reserved.
doi:10.1016/j.rse.2011.09.029

for the operational crisis management and mitigation. We shall evidence the new possibilities provided by the Sentinel-1 platform and sensor characteristics, for the improvements of these applications and for establishing new ones.

2. Using synthetic aperture radar interferometry (InSAR) to measure surface deformation

In this section we briefly introduce the SAR processing techniques used in geophysical applications; for a more detailed treatment of the subject we refer the reader to Bürgmann et al., 2000.

A SAR image contains a two-dimensional record of both the amplitude and the phase of the returns from targets within the imaging area. The amplitude stands for the reflectivity while the phase is a term proportional to the sensor-to-target distance. A particular SAR data processing technique referred to as InSAR (Interferometric SAR) is widely used in seismology, volcanology, hydrogeology, glaciology and subsidence studies. The InSAR approach aims at estimating any variation of the phase component of two or more SAR images taken under the same acquisition geometry. This means that the images need to be acquired along the same orbit, at different times (repeat-pass configuration). Since SAR is a coherent sensor, the phase information of any SAR image is related to the sensor-to-target distance. The interferogram, i.e. the result of the interferometric processing, is generated by computing the phase difference of two radar images on a pixel-by-pixel basis. Indeed, satellite SAR sensors can acquire new data over the same area of interest, using the same acquisition geometry, many times a year, thus allowing a comparison of the phase maps at different times. In repeat-pass interferometry, the temporal baseline is the time difference between two SAR acquisitions, the minimum temporal baseline corresponds to the satellite "repeat-cycle" (or revisit time) and varies from 11 days to 46 days for the satellites available today. Using satellite constellations, the actual revisit time can be further reduced to only few days.

The interferometric phase ϕ_{int} can be schematically split into five terms, the "flat Earth" component ϕ_f, the topographic phase ϕ_{topo}, the displacement phase ϕ_{displ}, the atmospheric term ϕ_{atm} and the error phase ϕ_{err} (Bürgmann et al., 2000). Except for the last, each term contains information relevant to specific issues, but for the applications described in this paper the signal of interest is ϕ_{displ}, i.e. the phase variation due to changes in the sensor-to-ground distance. The displacement phase (also called range change) is best shown in the differential interferogram, where the "flat Earth" and the topographic terms have been removed (the latter in general using an external Digital Elevation Model). The process of generating such topographically corrected interferogram is known as Differential InSAR (DInSAR). Although DInSAR is the actual processing technique used in most geophysical applications, the more general term InSAR is often used in the recent geophysical literature, implying in a way that interferograms are necessarily corrected for topography.

A further, fundamental step in InSAR analysis is the conversion of the original discontinuous, *modulo 2π* 'wrapped' interference signal, into an 'unwrapped' continuous phase signal, performed in the so-called 'unwrapping' process (e.g. Bürgmann et al., 2000). Phase unwrapping is often considered as a critical step in the estimation of ground displacement, and if an interferogram is largely affected by noise, the lack of signal continuity (decorrelation) may introduce errors in the displacement values (unwrapping errors). Such errors are usually accounted for using independent observations, such as GPS, leveling data, or other interferograms from different orbits or satellites.

After the DInSAR technique was consolidated, and became a tool for geophysicists rather than a research subject for electronic engineers, the research in SAR signal processing moved rapidly towards new developments. Taking advantage of the large numbers of images available in the ESA archives, the analysis focused increasingly on the investigation of the temporal evolution of the surface deformation. New SAR data processing techniques were developed to provide displacement time series for each ground point which could remain coherent over the entire multi-year data set (Berardino et al., 2002; Crosetto et al., 2005; Ferretti et al., 2000; Hooper et al., 2004; Mora et al., 2003; Usai, 2003; Werner et al., 2003).

The aim of all multitemporal techniques is to overcome some limitations of conventional InSAR, mainly phase noise (Zebker & Villasenor, 1992) and atmospheric effects (Zebker et al., 1997), taking advantage of long temporal series of SAR data. Rather than simply generating single interferograms and stacking them, these algorithms identify areas or individual ground targets where signal to noise ratio (SNR) values are favorable for InSAR measurements and generate time series of phase data where atmospheric disturbances can be characterised and removed. From the geophysical point of view, the main advantage of the multitemporal analysis is to generate the time history of the ground deformation, allowing a better understanding of the various processes acting in the seismic cycle.

At present, multitemporal techniques can be divided into two broad families of algorithms usually referred to as Persistent Scatterer (PSI), and Small Baseline (SBAS) approaches. In the following, we briefly describe the main features of both.

2.1. Persistent scatterer methods

The term Persistent Scatterer Interferometry defines techniques aiming at identifying individual scatterers exhibiting high phase coherence in all images of a multitemporal SAR dataset. The first PSI algorithm was the so-called Permanent Scatterer InSAR technique (PSInSAR), developed in the late Nineties at the Politecnico di Milano (Ferretti et al., 2000, 2001). Since then, many research centres and private companies have developed similar strategies for processing InSAR data-stacks.

A Permanent – or Persistent – Scatterer (PS) is defined as a radar target, within a SAR resolution cell, that displays stable amplitude properties and coherent signal phase, throughout all the images of a data stack. Objects that make good PS can be natural: rock outcrops, hard non-vegetated earth surfaces, single boulders, or man-made: buildings, light poles, transmission towers, metallic objects, walls and fences.

In the original PSI algorithm (Ferretti et al., 2000, 2001), all interferograms are generated using a single master scene, carefully selected within the available data-set of SAR scenes, in order to minimize temporal and geometrical decorrelation phenomena. In order to preserve the phase information related to isolated point-scatterers, interferograms are not filtered spatially. Initial PS selection is typically made by identifying scatterers that have consistently high amplitudes. Next, the time series of interferometric phases for each of these scatterers are unwrapped by considering the temporally correlated nature of deformation, usually assuming that the displacement time series can be well approximated with a low-order polynomial, possibly superimposed on a seasonal signal. Residual phase at each epoch is typically assumed to be tropospheric in origin; the residuals are interpolated and removed from each interferogram. A secondary search for further phase-stable pixels can then be made by considering the phase time series of each pixel, which are unwrapped in a similar way. Several variations on this algorithm have been implemented and used since the original algorithm was proposed; there are differences in particular in the methods used to unwrap the interferometric phase. For instance, in the StaMPS algorithm, the phase of each interferogram is unwrapped spatially, rather than by assuming a functional form for the time series (Hooper et al, 2004).

The most important factors impacting on PS data quality are:

- Spatial density of the PS (the lower the density, the higher the errors involved in estimating the tropospheric phase).

- Quality of the radar targets (signal-to-noise ratio levels).
- Ambient conditions at the time of the acquisitions (e.g. the amount of atmospheric turbulence and relative humidity).
- The distances between each measurement point and the reference point (similar to the case of differential GPS data, all measurements are differential measurements with respect to a reference point of known or assumed motion).

As a general indication, based on our experience and on a vast literature, using a satellite sensor with monthly repeat-cycle at mid-latitudes, it is possible to get an accuracy better than 1 mm/yr on a mean 3-year displacement rate for good radar targets located at less than 10 km from the reference point, assuming regular 35-day acquisition intervals as have been possible with the ERS-2 and Envisat satellites. Of course, the lower the satellite repeat cycle (i.e. the higher the temporal frequency of the observations), the shorter the time lag to get to the 1 mm/yr precision.

2.2. Small baseline methods

In contrast to PSI, SBAS algorithms enhance the SNR level of the interferograms through spatially averaging (locally) the phase values, to filter out the noise and to enable robust spatial phase unwrapping. Rather than selecting a single master scene for the generation of the interferogram stack as in the PSI methodology, multiple masters are used, with a fixed threshold on the maximum normal baseline value, limiting the impact of geometrical decorrelation (Zebker & Villasenor, 1992). Interferograms meeting the maximum baseline criterion are then generated, filtered, and unwrapped. Once all interferograms have been unwrapped, phase data are combined (usually via the Singular Value Decomposition) to estimate a displacement time series for pixels exhibiting a good coherence level in most of the interferograms (Berardino et al., 2002; Crosetto et al., 2005; Usai, 2003).

Although different versions of the algorithm exist, the SBAS approach is usually more efficient over distributed scatterers (i.e. wherever no dominant scatterer can be identified), rather than on pointwise targets and whenever the spatio-temporal distribution of the baseline values makes it possible to have a single set of small-baseline interferograms creating a connected graph with all the images of the data-set (Sansosti et al., 2010).

Recently, some new algorithms that aim to combine the advantages of PSI and SBAS techniques, have been presented (Ferretti et al., 2009; Hooper, 2008; Prati et al., 2010). These new approaches allow one to increase the spatial density of the measurement points and to obtain a better combination of the information coming from all the interferograms that can be generated from a long-term dataset. Current research foci include: the estimation and removal of tropospheric effects (Hobiger et al., 2010) which still represent a major limitation of any InSAR analysis; estimation and removal of residual orbital phase components (e.g. Biggs et al., 2007); and the exploitation of SAR data sets characterized by high spatial resolution and short repeat cycles, provided by new satellite constellations (Lanari et al., 2010).

3. Observing the seismic cycle using InSAR

The concept of the seismic cycle (also known as the earthquake cycle) is born from the observation that earthquakes can occur repeatedly on the same segments of faults, over time scales that are typically decades to centuries in length. In each individual seismic cycle, the rapid and large surface displacements that accompany an earthquake are typically preceded by a long period of slow, gradual loading, and followed by a shorter, transient period of rapid deformation; we therefore subdivide the seismic cycle into three phases. We call the loading phase, where strain accumulates on the fault segment(s), the *interseismic* phase. InSAR observations of this phase can make important contributions to the assessment of seismic hazard, as the rate of strain accumulation on a fault can be directly related to the rate of earthquake recurrence. Once sufficient strain has been accumulated such that shear stress on the fault exceeds a fault's frictional strength, an earthquake occurs; we call this the *coseismic* phase of the seismic cycle. Studies of this phase of the seismic cycle can lead to improved knowledge of earthquake source processes. Finally, after the earthquake, we enter the *postseismic* phase. In this interval, the stress changes that were imparted by the earthquake are relaxed, typically stimulating movement in the subsurface at rates that, while slower than earthquake motions, are significantly faster than interseismic rates. Study of this period of the seismic cycle can lead to understanding of the constitutive laws and parameters of the crust and uppermost mantle, fundamental to our understanding of how the lithosphere responds to stress. All three phases of the seismic cycle have been studied using InSAR data; we will discuss each of them in turn.

3.1. Interseismic deformation

Measuring interseismic deformation with InSAR is challenging – typically, rates of deformation are small (<3 cm/yr), and the deformation signal can be distributed over tens of kilometres. Interferograms that aim to capture such deformation are therefore susceptible to noise, errors and often decorrelation. A small displacement signal can be masked by the effects of differential tropospheric water vapour – the principal source of 'noise' in interferograms of deformation. In areas that contain significant amounts of vegetation, it is not possible to increase the deformation signal (and thus improve the signal to noise ratio in the data) by simply increasing the time span of the interferogram – this will increase the probability of temporal decorrelation in the interferogram, and thus reduce the number of useable pixels. Finally, the length scale of interseismic deformation signals is similar to that of long-wavelength gradients due to incorrect determinations of satellite orbital position; consequently, estimates of the strain accumulation rate, and therefore the geodetic 'slip rate' associated with the fault, can be erroneous.

Several strategies have been employed to improve the likelihood of recovering interseismic deformation from InSAR data. One method is interferogram stacking – averaging a number of interferograms so that random tropospheric noise is reduced. There are two approaches in stacking that have been shown to work well–either the very best data can be stacked (the 'quality' approach), or larger volumes of data are used (the 'quantity' approach). In an example of the former, Wright et al. (2001) stacked four independent interferograms identified as having low tropospheric water vapour content and minimal residual orbital gradients in order to determine the geodetic slip rate of the North Anatolian fault in eastern Turkey. In an example of the latter, Peltzer et al. (2001) stacked 25 interferograms from the Eastern California Shear Zone, using GPS data as an additional constraint so that the long-wavelength orbital errors could be estimated and removed. Similar approaches have since been applied over a number of different tectonically active fault systems, such as the faults in western Tibet (Wright et al., 2004a), central Tibet (Taylor & Peltzer, 2006), and the southern San Andreas fault (Fialko, 2006). More recently, multitemporal approaches such as those described in Section 2, have been successful for clarifying interseismic deformation signals from sets of noisy interferograms (Cavalié et al., 2008; Fialko, 2006; Hunstad et al., 2009).

Models that are used to interpret these data range from simple 1-D analytical models developed for the analysis of trilateration data (e.g. Savage & Burford, 1973), through three dimensional dislocation models (e.g. Okada, 1985), to models of deformation over networks of faults (e.g. Schmidt et al., 2005). Some groups have attempted to use such models as prior information on the form of a multitemporal interferogram rate map, assisting with interferogram unwrapping

and the estimation of improved orbital corrections. Biggs et al. (2007) used such a hybrid model/small baseline subset method to jointly estimate the fault slip rate, regional deformation rates and orbital corrections using interferograms covering the Denali fault in Alaska, an area where simple stacking provided insufficient constraints on the deformation model on its own (Fig. 1).

3.2. Coseismic deformation

The first application of InSAR to an earthquake dates back to 1992, when the surface displacement field due to the Landers earthquake was clearly detected and measured using a pair of ERS1 images (Massonnet et al, 1993). The Landers coseismic image pair, spanning April 24 – August 7, 1992, provided the optimum conditions for coherence thanks to the short temporal baseline, a minimal difference in orbital position between the two images and the arid desert surface with minimal vegetation. In subsequent years, thanks to the long-sighted ESA policy of background data acquisition, the constantly increasing ERS image archive provided the necessary data for similar applications in a wide variety of environments and acquisition conditions as the 1994 Northridge earthquake (Massonnet et al., 1996), 1995 Dinar earthquake (Wright et al., 1999) and 1997 Umbria-Marche earthquakes (Lundgren & Stramondo, 2002; Salvi et al., 2000; Stramondo et al., 1999). At the time of writing, over 60 earthquakes, with magnitudes between 4.4 and 8.5 have been studied with InSAR (see Weston et al., 2011).

InSAR offers many advantages in the study of the earthquake source, particularly in areas where coherence is good. For instance, InSAR allows a precise determination of the geometries of the fault segments involved in an earthquake. The surface rupture geometry and length can often be mapped directly from the data. Additionally, through consideration of simple elastic dislocation models (e.g. Okada, 1985), certain specific features of the deformation pattern can be related to other earthquake source parameters: for instance, asymmetry in the deformation pattern can provide information on the dip and rake of the fault responsible; the fault-perpendicular extent of the deformation pattern is related to the bottom depth of the fault; the magnitude of the surface displacement is related to the magnitude of fault slip. Typically, a nonlinear optimization algorithm is used to modify analytical elastic dislocation models to search for the set of earthquake source parameters that give the best match to the observed displacements (e.g. Lohman et al., 2002; Wright et al., 1999). Often these geometric parameters are better constrained by InSAR data than by other data (e.g. Funning et al., 2005a,b).

Once a geometry for the fault is obtained, the fault segments are typically subdivided into smaller subfaults, or 'fault patches'. For a fixed fault geometry, the relationship between fault slip and ground displacement, e.g. as measured by InSAR, is linear, meaning that it is trivial to invert for the slip on each fault patch (e.g. Feigl et al.,

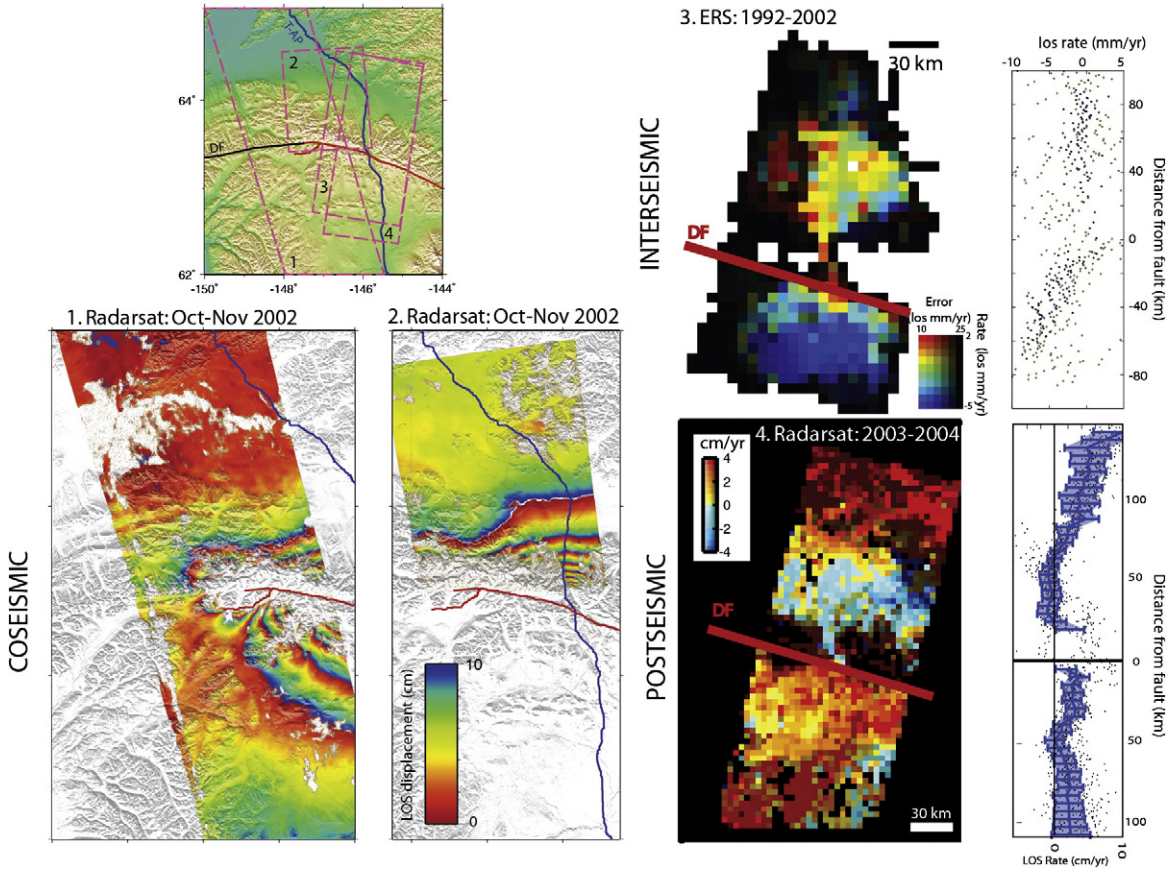

Fig. 1. Elements of the seismic cycle as observed using InSAR on the Denali fault (DF), Alaska. Top left: Map showing the location of: portions of the DF that ruptured in the 2002 earthquake (red); unruptured portions of the DF (black); the Trans-Alaska Pipeline (T-AP, blue); the locations of SAR frames (pink dashed lines). Top right: Interseismic deformation rate map for the Denali fault generated from 44 descending track ERS SAR interferograms from data acquired between 1992 and 2002. Shading indicates the level of uncertainty in the rates; these are lowest close to the Trans-Alaska Pipeline which is coherent in most of the interferograms. The rate map data are consistent with a geodetic slip rate of 11 ± 5 mm/yr (after Biggs et al., 2007). Bottom left: Example coseismic interferograms generated from ascending track Radarsat data acquired a few weeks either side of the 3 November 2002 M7.9 Denali earthquake (after Wright et al., 2004b). Bottom right: Postseismic deformation following the Denali earthquake, estimated using 41 Radarsat interferograms. Note that deformation rates are close to an order of magnitude faster than the interseismic rates (after Biggs et al., 2009).

2002; Funning et al., 2005a; Jónsson et al., 2002; Simons et al., 2002). In such studies, it is usually necessary to regularize the inverse problem (i.e. reduce the number of independent model parameters) by adding smoothing constraints, typically a finite-difference Laplacian constraint (e.g. Jónsson et al., 2002).

The accurate and spatially dense InSAR measurements of the coseismic deformation has given the possibility to model fault dislocations with a detail often not obtainable with any other means. Inversion of the displacement data allows to map the rupture geometry and sense of movement with high accuracy, especially when multiple interferograms from different sensors and viewing geometries are used (Atzori et al., 2009; Wright et al., 2003, 2004). As will be shown in Section 4, these data can have important application in the operational management of a seismic crisis.

3.3. Postseismic deformation

Postseismic displacement has been detected and measured by InSAR since 1992, when Massonnet et al. (1994) concluded that most of the post-earthquake movements of the Landers strike slip event were concentrated in the 40 days after the mainshock. Ongoing observations have subsequently shown that deformation continued for several years after the event (Fialko, 2004). In subsequent years, several more earthquakes have generated postseismic displacements detectable with InSAR, including Manyi in 1997 (Ryder et al., 2007), Hector Mine in 1999 (e.g. Jacobs et al., 2002; Pollitz et al., 2001), Izmit in 1999 (e.g. Bürgmann et al., 2002; Ergintav et al., 2002; Hearn et al., 2002) and Denali in 2002 (Biggs et al., 2009; Pollitz, 2005). These postseismic movements are the response of the lithosphere to stresses imposed by the earthquake. An active area of current research is to explain how and where the stresses are relaxed, and by what mechanism. Postseismic displacements have been modelled as afterslip on a discrete plane (e.g. Bürgmann et al., 2002), creep in a viscous or viscoelastic shear zone (e.g. Hearn et al., 2002), viscoelastic relaxation in the lower crust/upper mantle (e.g. Pollitz et al., 2000), and poroelastic rebound (e.g. Jonsson et al., 2003). In some cases, it is likely that multiple mechanisms are operating, often with different time constants – poroelastic rebound coupled with localised deep shear (e.g. Fialko, 2004); poroelastic rebound, afterslip and shallow volumetric contraction (Fielding et al., 2009).

The use of InSAR in the study of postseismic movements in the subduction areas has led to improve the comprehension of the source mechanism in such transitional zones (Béjar-Pizarro et al., 2010) characterized by alternating transient aseismic shear and seismic slip (Hyndman & Wang, 1993). Transient aseismic slip is also observed as postseismic afterslip in both the lower region and the upper region of the seismogenic zone (Fig. 2), thus apparently in areas surrounding the main asperity characterized by high coseismic slip (e.g. Baba et al., 2006; Chlieh et al., 2004; Hsu et al., 2006; Miyazaki et al., 2004; Pritchard et al., 2006). Postseismic deformation time series over normal faults have also been estimated using multitemporal analysis: during the 1999 Athens earthquake (Atzori et al., 2008) using 26 + 47 ERS images from ascending and descending orbits, and during the 2009 L'Aquila earthquake, using a data set of 32 X-band COSMO-SkyMed images acquired in the 8 months after the mainshock (Lanari et al., 2010).

3.4. Limitations of InSAR in studies of the seismic cycle

Scientific research based on InSAR data has been limited until now by some relevant technical drawbacks. The main limits coming from the satellite systems available up to few years ago (ERS, ENVISAT, JERS, RADARSAT, ALOS) concerned the long revisit time intervals (a minimum of 24 to 46 days depending on mission). Often, the repeat time between acquisitions has been a multiple of the minimum repeat time, due to limitations in onboard data storage and power supply, and acquisition conflicts – in most of the currently operating SAR satellites it is not possible to acquire images over every point on every orbit. This has in general limited the use of SAR Interferometry to areas characterised by stable surfaces (urban, rocky, or arid environments) where the surface scattering properties change very slowly with time. Moreover, for conventional InSAR analyses, the long revisit

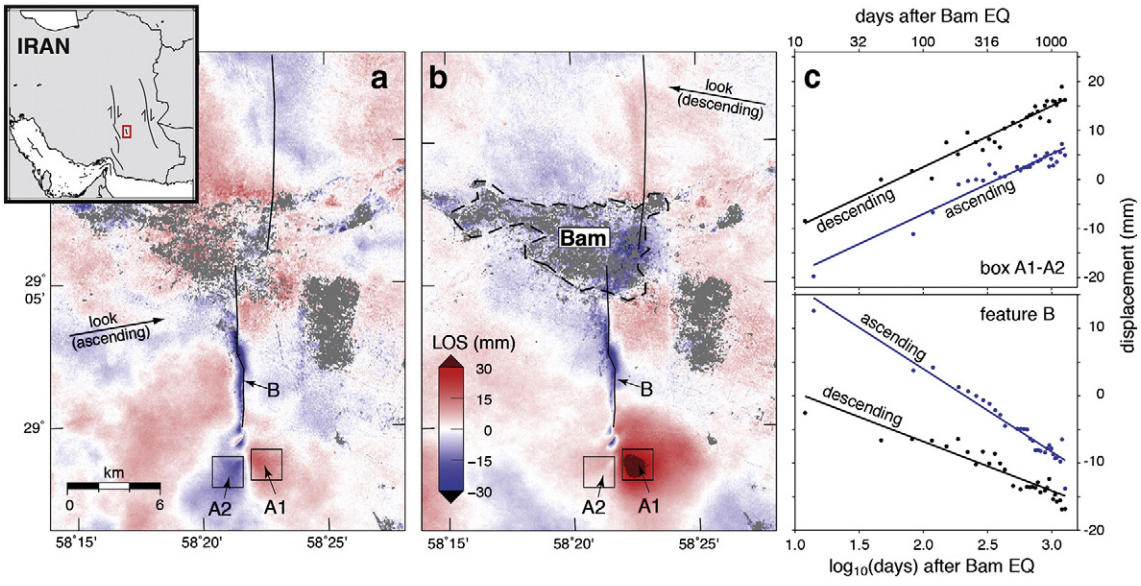

Fig. 2. Spatial and temporal patterns of postseismic deformation following the 2003 Bam, Iran earthquake. (a) Total LOS displacement that occurred between 12 and 1097 days after the earthquake (January 2004–December 2006) from ascending track 156 data. (b) Total LOS displacement for the same time period from descending track 120 data. Solid black line shows the location of the Bam fault. Dashed black line shows the location of the city of Bam; decorrelation within that area is mostly due to palm vegetation and the city reconstruction. (c) Log-linear plots of the time dependence of two deformation features seen in the two data sets. 'Box A1–A2' shows the cross-fault signal at the southern end of the Bam fault, obtained by differencing data from either side of the fault trace (boxes A1 and A2 in (a) and (b)). In the descending data this difference is consistently smaller than in the ascending data, implying a significant component of E–W horizontal motion; this is interpreted as the effect of afterslip at the end of the fault segment at 2–3 km depth. 'Feature B', obtained by differencing data from the fault trace (feature B in (a) and (b)) with nearby data, shows a subsidence feature centered on the fault trace, interpreted as fault-zone dilatancy recovery. In both cases, deformation follows a straight line trend in log-linear space, implying a logarithmic decay in the deformation over time. Inset map shows location of the area of interest within SE Iran. After Fielding et al., 2009.

time implies a sparse temporal sampling of the ground displacements, which can affect the significance of the modeling. For instance, interferograms of coseismic displacement fields created using temporally distant images, may contain an unknown amount of postseismic deformation, with an impact on the source parameter estimation. In fact, during the whole lifetime of the ERS and ENVISAT satellites, only in very few cases has a timely post-event image acquisition occurred: the Umbria-Marche, 1997 (few minutes time delay, Salvi et al., 2000), and the Hector Mine, 1999 (4 days time delay, Sandwell et al., 2000) earthquakes, being two examples.

Some of the SAR instruments from the old generation, with low resolution and low revisiting time are no longer operative (see ERS-1, ERS-2 and JERS-1) or are close to the end of their operation (Radarsat-1 and ENVISAT). During the last 8 years, the ENVISAT mission has been the main source of SAR data for scientific research, but at the end of October 2010 the satellite orbit had to be lowered to ensure extension of the mission up to 2013. The orbit change resulted in a general increase of the spatial baselines, to an extent that will prevent the building of multitemporal InSAR data sets for most areas of the world. Only for images acquired within two narrow bands centered at $+-38°$ latitude, will the baselines be low enough to form useful interferometric pairs over several cycles.

Since 2007, with the Japanese ALOS PALSAR, the first HR (High Resolution) SAR system operating at L band became available, characterized by a larger revisiting time than the existing C-band systems (46 days), but also by a better potential for InSAR applications, as the L-band SAR data are significantly less affected by temporal decorrelation (Bürgmann et al., 2000). Also in 2007, the Canadian Space Agency launched the Radarsat-2, carrying a C-band sensor capable of different acquisition modes, spatial resolution up to 3 m and full polarimetric capabilities. The most recent SAR missions are both based on X-band, VHR (Very High Resolution) imaging systems: the German TerraSAR-X, achieving 1 m resolution and 11 days revisiting time (Werninghaus, 2006) and the Italian COSMO-SkyMed, 1 m resolution and 4 days revisiting time in InSAR mode (Caltagirone et al., 2007).

4. Operational applications for seismic risk management

The significant advances in solid earth geophysics promoted by ERS and ENVISAT data have had important benefits for the society. The new observations of crustal strain accumulation and release during the seismic cycle, and the analysis they have fostered, allowed a better knowledge of many active faults, eventually resulting in improvements of regional Seismic Hazard Assessment (SHA). However, there are other uses of SAR data in the decision-making chain of seismic risk management, which have been so far only partially demonstrated, and which can be boosted by Sentinel 1 data.

In the following we discuss the possibility of an operational use of InSAR data in the risk management phases named *Knowledge and Prevention*, and *Warning and Crisis* (Beer & Ismail-Zadeh, 2002; Lettieri et al., 2009). Most of the following discussion is based on the results of the SIGRIS project (2008–2010), funded by the Italian Space Agency. This has been the first project aiming to demonstrate the potential of present and future SAR and optical satellite systems for operational activities in seismic risk management (Salvi et al., 2010). A complex infrastructure has been developed for the acquisition, storage, management, processing, modeling and interpretation of satellite data, integrated with the seismic monitoring activities of the INGV National Earthquake Center. The various products (maps, models, reports) generated by the SIGRIS system have been evaluated and approved by the Italian Civil Protection Department, the state-wide agency for seismic risk management in Italy.

The Knowledge and Prevention phase of seismic risk management comprehends all activities concerning the risk assessment, mitigation and preparedness. They are carried out before the earthquake occurs, and are presently the only effective way to reduce the impact of earthquakes on the society, since earthquake prediction will not be a reality for several decades, if ever (Geller, 1997; Geller et al., 1996; Jackson et al., 1997). As mentioned before, Seismic Hazard Assessment has been the main application field of the new scientific results obtained through ERS/ENVISAT data and the use of InSAR and multitemporal InSAR, in particular for the parameterization of the seismic sources (Fielding et al., 2004; Xinjian & Guohong, 2007), for the definition of the present deformation rates (Bürgmann & Prescott, 2000; Funning et al., 2007; Hunstad et al., 2009; Lyons & Sandwell, 2003; Motagh et al., 2007; Nof et al., 2008), for the partitioning of strain among different faults (Jackson et al., 2006), for the improvement of tectonic models in seismogenic areas (Biggs et al., 2006; 2007). Most of these studies have been possible thanks to the longsighted ESA policy of maintaining repeat image acquisitions over many seismically active areas worldwide (the so-called "background mission"). Now that new InSAR analysis techniques have been developed and made progressively more available to geophysicists, this enormous amount of data is showing its large potential for the monitoring of the strain accumulation along active fault zones. The geodetic data are then used to model the long-term interseismic slip rates which, together with the geological slip estimates and seismological data, are used to quantify the known earthquake sources in probabilistic SHA (Hearn et al., 2010; Petersen et al., 2007). Still, to promote a better and more effective use of scientific results arising from interseismic deformation studies, in Seismic Hazard maps, some practical issues have to be addressed. These include standardization of procedures for the SAR data analysis (especially multitemporal InSAR analysis) and uncertainty determination, development of standard (or consensus) modeling procedures, a thorough assessment of significance and uncertainty of model results.

The Warning and Crisis phase of seismic risk management concerns all activities needed to promptly and effectively respond to the effects of an earthquake, usually with a priority on the effects on the human environment. The first piece of information needed after a large earthquake occurs is an assessment of the extent and intensity of the earthquake impact on man-made structures, immediately after which it becomes important to formulate hypotheses on the evolution of the seismic sequence, i.e. where local aftershocks or future mainshocks (on nearby faults) may be expected.

Much research has been done on earthquake damage assessment using remote sensing data (Sakamoto et al., 2004), and the all-weather imaging capability of SAR data are certainly a valuable asset (Matsuoka & Yamazaki, 2002; Yonezawa & Takeuchi, 2001) with respect to HR optical imagery. The use of SAR remote sensing for damage detection after destructive earthquakes has been proposed (Matsuoka & Yamazaki, 2001; Matsuoka & Yamazaki, 2004), and applied retroactively (e.g. Fielding et al., 2005) but has not been considered as an operational opportunity, mainly due to the strict temporal constraints of the application.

We estimate that an earthquake damage map obtained from remote sensing data can be outdated by ground surveys in a time frame between 2 and 10 days, depending on earthquake magnitude and social/environmental context. In fact, damage areas of moderate magnitude earthquakes (M_w 5.8–6.4) occurring in developed countries, could be effectively surveyed by ground teams or aerial means in a couple of days, while for undeveloped regions and earthquakes with $M_w > 7$ (damage areas of several hundreds of km^2) several days may be needed to obtain a synoptic damage map. Clearly the best-case, 35-day revisit interval of ERS/ENVISAT (or the slightly smaller ones of other SAR systems) was too large to match these requirements regularly. This drawback could be reduced, in an operational perspective, by combining data from different sensors, and good results have been obtained by the joint use of SAR and VHR optical remote sensing systems (Stramondo et al., 2006). Still, the best operational configuration would be based on high resolution SAR imagery, and a constellation of satellites capable of flexible and very

short revisit intervals. Presently the only system with these characteristics is the Italian COSMO-SkyMed constellation of 4 satellites with a high resolution, X-band SAR (Caltagirone et al., 2007). In fact, COSMO-SkyMed is the first constellation of SAR satellites specifically designed for an operational use in defense and in civilian applications, as monitoring of environmental resources and risk management.

The potential of COSMO-SkyMed HR SAR data for early damage assessment was demonstrated after the 2009 L'Aquila earthquake using a postseismic image acquired 3 days after the event and two acquired within 1.5 months prior to the event (Dell'Acqua et al., 2011).

Another very important piece of information in seismic crisis management is the so-called "event scenario", whose goal is to provide the authorities in charge with some important elements to address, for instance, the choice of emergency housing locations, evacuation strategies, or specific safety measurements for man made structures. In an event scenario an assessment of the short-term spatial evolution of the seismic sequence may be attempted, even if likely affected by large uncertainties, due to the knowledge gaps still existing in earthquake dynamics (Steacy et al., 2005).

Important elements of an event scenario are:

- Location and assessment of the seismic source.
- Location and assessment of induced hazards (fault scarps, landslides, soil liquefaction areas, ground displacement areas).
- Estimates on short term spatial evolution of the seismic sequence.

4.1. Location and assessment of the seismic source

As shown in Section 3 of this paper, there has been much research on the analysis of the seismic source by modeling the static coseismic surface displacement measured through InSAR. Unless more complicated elastic structures need to be taken into account (Masterlark, 2003) the source modeling is a straightforward process, carried out using analytical solutions for dislocation in an elastic, homogeneous crust. The inversion procedures described in Section 3 can be rather fast (1–2 h) and, yet they have not become part of the operational seismic source assessment carried out by seismological services (as for instance have been the Centroid Moment Tensor and source time function estimations). This is mainly due to the unpredictable availability of timely SAR data and to the variable level of interferometric coherence. When SAR data are made available in near-real time, as for COSMO-SkyMed imagery during the 2009 L'Aquila earthquake (Central Italy), seismic source models can be continuously generated and updated during the seismic sequence, and rapidly released to the Civil Protection authorities (Salvi et al., 2009). During the L'Aquila crisis, the SIGRIS system generated and released 5 different source models, using postseismic images acquired as little as 3 days after the mainshock. The L'Aquila fault rupture did not generate massive surface faulting, and the models constrained by InSAR allowed the timely and precise identification of the Paganica fault as the earthquake source (Atzori et al., 2009).

4.2. Location and assessment of induced hazards

The coseismic surface displacement maps obtained by InSAR do not contain only the signal due to the coseismic fault slip. Often local signals can be appreciated, due to gravitational deformations induced by the seismic ground motion. The accurate mapping and quantification of these phenomena is a priority for Civil Protection authorities, especially in densely populated areas (Yin et al., 2009). Again, a rapid assessment of these induced hazards is feasible when SAR data are acquired and distributed in a timely fashion (Moro et al., 2007; Moro et al., 2011).

4.3. Estimates on short term spatial evolution of the seismicity

It is now widely accepted that stress changes (both static and dynamic) caused by large earthquakes in the Earth's crust, can trigger or anticipate seismic slip on other faults (King et al., 1994; Parsons & Dreger, 2000; Stein, 1999). Presently several methods to relate the spatial distribution of aftershocks to Coulomb stress changes induced by the mainshock, have been proposed (see a review in Steacy et al., 2005). All require that the source geometry be known, and most need also a well constrained distribution of slip on the fault plane. Therefore, a quick and accurate assessment of the seismic source as can be obtained by space geodetic data, and DInSAR interferograms in particular, is the basic requirement to attempt estimates on the short term evolution of aftershocks. Although the methods are still under study, and no standard procedure exists to date, the information coming from even an uncertain aftershock forecast may prove very useful during emergency response (McCloskey & Nalbant, 2009). Moreover we expect that improved monitoring capacities, able for instance to generate rapid and repeatedly updated maps of surface displacement, will foster further analyses in this field.

5. Sentinel-1: the European Radar Observatory

Building on the experience of the ERS and ENVISAT Earth observing satellites, and in compliance with the operational requirements of the Global Monitoring for Environment and Security Programme (GMES) space segment, ESA has developed the Sentinel concept for a constellation of operational satellites, each one focused on specific applications (ESA, 2010). The first mission will be Sentinel-1, also called the European Radar Observatory, a polar-orbiting satellite system hosting C-band SARs. The first satellite (Sentinel-1A) is due to be launched at the end of May 2013, followed by a second satellite (Sentinel-1B) within the following two years. Sentinel-1A and -1B are part of the European contribution to the Global Earth Observation System of Systems (GEOSS).

The Sentinel-1 mission will ensure the continuity of SAR C-band missions, building upon ESA's and Canada's heritage with SAR systems onboard ERS-1, ERS-2, Envisat, and Radarsat-1 and -2. Among many other applications, the Sentinel-1 mission and its data will give the possibility of detecting, measuring, modeling and monitoring ground displacements (e.g. for earthquake and volcano studies) in the order of a few mm, by the implementation of InSAR techniques.

The Operational Modes of the satellite will be:

1. A Stripmap Mode (SM) with 80 km swath and 5×5 m spatial resolution, with generally restricted use, mainly for emergency purposes.
2. An Interferometric Wide swath Mode (IW) with 250 km swath and 5×20 m spatial resolution (range and azimuth respectively), obtained through burst synchronisation; this will be the preferred mode over land areas, used almost routinely for interferometry and hence of particular interest for geophysical applications.
3. An Extra-wide Swath Mode (EW) with 400 km swath and 25×40 m spatial resolution, mainly for sea-ocean applications.
4. A Wave Mode (WM), for open ocean applications, acquiring in leap frog mode imagettes of 20x20 km every 100 km along the orbit, with 5x5 m spatial resolution and alternating 23° and 36.5° incidence angles.

Sentinel-1A will have a 12-day revisit time, which will improve to a 6-day effective repeat cycle after the launch of the twin satellite Sentinel-1B, potentially allowing a weekly monitoring of deformation phenomena over the major seismic areas of the world at intermediate latitudes. Effective revisit time at high latitude areas will possibly be as short as 1 day (Snoeij et al., 2010).

The higher temporal frequency of observation compared to C-band sensors available today, as well as the planned regularity of the acquisitions over the areas of interest will allow a more accurate quantification of deformation rates for both classical InSAR and multitemporal techniques. A higher spatial density of measurement points is expected to result (Lanari et al, 2004) from a more effective filtering of the atmospheric components and a lower impact of temporal decorrelation phenomena. The interferometric coherence will be improved not only for the more frequent and regular acquisitions, but also thanks to a tighter orbital control (thus decreasing geometric decorrelation) which will maintain the orbital tube (i.e. the maximum perpendicular baseline) within 100 m.

It is expected that Sentinel-1 data will allow strong improvements in all applications described in this paper. The time necessary to create an interferometric data-stack suitable for multitemporal analyses of ground deformation (a minimum of ~20 images) will be strongly reduced (8 months compared with >2 years). The higher monitoring frequency of rapidly evolving deformation phenomena (as in the early postseismic phase) will be useful to develop improved models of stress transfer across faults, with evident benefits on operational applications. The more rapid sampling and improved interferometric coherence of Sentinel-1 data should also increase the possibility of multitemporal analysis in areas with less stable surfaces and more changeable environmental conditions. The limited orbital deviation across different passes shall guarantee small perpendicular baselines in all interferometric pairs, favouring multitemporal analyses based on the Small Baseline techniques. The 250 km-wide swath of the IW mode will provide the capability to observe slow deformation phenomena, such as interseismic strain accumulation or postseismic relaxation, over large areas, allowing to better separate deformation signals from orbital fringes. Finally, another SAR-based technique, currently used in geophysics, which will benefit from the Sentinel-1 enhanced capabilities is the use of speckle correlation for fault rupture detection and for 2-D ground deformation monitoring (see Deraw, 1999; Gray et al., 1998; Sarti et al., 2006). The reduced revisit time and the smaller geometrical baseline values imply a better speckle preservation that will enhance the correlation performances.

6. Operational use of Sentinel-1 data for monitoring the seismic cycle

The development of Sentinel-1 was undertaken as part of the GMES space segment, therefore the mission requirements were built on the basis of the outcomes of the GMES services developed at the EU and ESA level (Snoeij et al., 2010). The most important requirements for operational services (in different sectors) were: the continuity and certainty of data supply, a short revisit interval, a large geographical coverage, a rapid data distribution, and last but not least, a low data price. All these requirements have been fulfilled, and the Sentinel-1 constellation has the potential to stimulate the market development of many sustainable services. Using these data, it will become possible to develop services for the monitoring of the seismic cycle, although they will probably be carried out by academic establishments and government agencies, and not by commercial companies (as for seismic and geodetic monitoring activities). In fact we expect that the analysis of Sentinel-1 data will become part of the routine activities carried out by national and international agencies involved in earthquake research, earthquake hazard assessment, and civil protection activities.

During the ERS/ENVISAT era, even if a considerable effort was carried out by ESA, not all seismically active area of the world were systematically covered, whereas others, for technical constraints, did not attain a sufficient number of images for effective deformation analysis; moreover in many locations only a single acquisition geometry was well covered, while deformation is best estimated using both ascending and descending geometries. The so-called Background Regional Mission (BRM) planning, which was the default acquisition planning for ENVISAT/ASAR high resolution modes (Image, Wide Swath and Alternating polarization), defined an acquisition strategy with the aim to build up consistent data sets of scientific interest over areas where terrain movements occur (the so-called Strategic Data Sets – SDS), establishing some compromises between data requests from all the users.

The Sentinel-1 data acquisition strategy is instead devised for operational applications, and it is based on systematic, routine and conflict-free acquisitions, that are defined a-priori and will not be dynamically modified as a function of user requests. Over land, and in particular over active seismically or volcanic areas, data will be acquired in Interferometric Wide swath mode (IW) with 250 km swath and 5×20 m of spatial resolution (in range and azimuth respectively). This will allow effective coverage for interferometric data in a systematic way over InSAR relevant areas at global level, with a minimum revisit of 12 days with one satellite, and 6 days with both.

In less than a year it will become possible to build a data-stack large enough to use the multitemporal techniques mentioned in Section 2 for the mapping of slow deformations, possibly improving the measurement accuracies to below 1 mm/yr. The larger swath (it is 100 km for ERS/ENVISAT) could help to isolate areas of no deformation in the images, allowing a better separation among different signals (tectonic, orbital, ionospheric); the larger area will facilitate also the integration with Continuous GPS measurements of ground deformation, which will help to cope with a presumably higher error propagation.

The constant acquisitions will make possible to create the necessary archives for reliable mapping of coseismic displacement fields and the generation of detailed models of the seismic source, within only a few days of an earthquake. Maps of the heavily damaged urban districts and of locally triggered gravitational deformations will also be generated. All these value-added information products will be updated at each new acquisition, and released in incremental versions to the civil protection agencies.

The lack of standard procedures for product generation and distribution has been, in our experience, a major factor to limit the assimilation of these important information in civil protection activities during seismic crises. The certainty of data acquisition and constant flow of data provided by the Sentinels will allow to overcome such limitations.

Finally, we evidence that the Sentinel-1 mission will also allow Emergency Data Requests which can be inserted into the mission plan update at short notice. The system is designed in such a way that these emergency requests will have a minimum impact on the operational duty cycle (Snoeij et al., 2010).

7. Conclusions

Starting from the 1990s, the InSAR data have played and increasingly important role in the analysis of ground deformations. During the last two decades the constant refinement of the InSAR processing techniques has allowed a full exploitation of the large information content of the SAR data, contributing to improve our knowledge of the tectonic strain accumulation and release during the seismic cycle.

Among the new European operational satellites, the Sentinel-1 SAR mission will be the first to be developed, acknowledging the important successes obtained through ERS and ENVISAT data. The system has been designed to overcome most of the limitations evidenced by previous satellites, and its capacity to provide excellent data for SAR Interferometry is guaranteed by the small orbital tube and by the limited revisit interval. The latter could be further reduced in the future, just by adding new satellites to the constellation.

Sentinel-1 will also improve the already successful ERS/ENVISAT data policy and acquisition strategy, which allowed scientists worldwide easy access to consistent data archives for most tectonically active areas of the world. It is currently foreseen that the Sentinel-1 data could be free for scientific AND commercial use, and the flow of data will be constant and certain for a long period of time. All these

premises will ensure to Sentinel-1 the capacity to stimulate not only new scientific advances and stable commercial applications, but also services of relevant public interest, as in the hazard assessment and civil protection sectors.

Acknowledgements

P. Potin (ESA/ESRIN) is gratefully acknowledged for providing updated information and insights on the Sentinel missions. Many thanks are also addressed to F. Constantini (Tor Vergata University) for the constructive discussions and to two anonymous referees.

The SIGRIS pilot project has been funded by the Italian Space Agency in the framework of the national space plan, to promote the operational use of Earth Observation data for Seismic Risk Management.

References

Adam, N., Parizzi, A., Eineder, M., & Crosetto, M. (2009). Practical persistent scatterer processing validation in the course of the Terrafirma project. *Journal of Applied Geophysics*, *69*, 59–65.

Atzori, S., Hunstad, I., Chini, M., Salvi, S., Tolomei, C., Bignami, C., et al. (2009). Finite fault inversion of DInSAR coseismic displacement of the 2009 L'Aquila earthquake (Central Italy). *Geophysical Research Letters*, *36*(15), 305 [L15].

Atzori, S., Manunta, M., Fornaro, G., Ganas, A., & Salvi, S. (2008). Postseismic displacement of the 1999 Athens earthquake retrieved by the differential interferometry by synthetic aperture radar time series. *Journal of Geophysical Research*, *113*, B09309, doi:10.1029/2007JB005504.

Baba, T., Hirata, K., Hori, T., & Sakaguchi, H. (2006). Offshore geodetic data conducive to the estimation of the afterslip distribution following the 2003 Tokachi-oki earthquake. *Earth and Planetary Science Letters*, *241*, 281–292.

Beer, T., & Ismail-Zadeh, A. (2002). *Risk Science and Sustainability, NATO Science Series II, 112.* : Kluwer Acad. Pub1-4020-1446-5.

Béjar-Pizarro, M., Carrizo, D., Socquet, A., & Armijo, R. (2010). Asperities and barriers on the seismogenic zone in North Chile: State of the art after the 2007 Mw 7.7 Tocopilla earthquake inferred by GPS and InSAR data. *Geophysical Journal International*, *183*, 390–406.

Berardino, P., Fornaro, G., Lanari, R., & Sansosti, E. (2002). A new algorithm for surface deformation monitoring based on small baseline differential SAR interferograms. *IEEE Transactions on Geoscience and Remote Sensing*, *40*, 2375–2383.

Biggs, J., Bergman, E., Emmerson, B., Funning, G. J., Jackson, J., Parsons, B., et al. (2006). Fault identification for buried strike-slip earthquakes using InSAR: The 1994 and 2004 Al Hoceima, Morocco earthquakes. *Geophysical Journal International*, *166*(3), 1347–1362.

Biggs, J., Bürgmann, R., Freymueller, J. T., Lu, Z., Parsons, B., Ryder, I., et al. (2009). The postseismic response to the 2002 M 7.9 Denali Fault earthquake: constraints from InSAR 2003–2005. *Geophysical Journal International*, *176*, 353–367, doi: 10.1111/j.1365-246X.2008.03932.x.

Biggs, J., Wright, T., Lu, Z., & Parsons, B. (2007). Multi-interferogram method for measuring interseismic deformation: Denali Fault, Alaska. *Geophysical Journal International*, *170*, 3, doi:10.1111/j.1365-246X.2007.03415.x.

Bürgmann, R., Ergintav, S., Segall, P., Hearn, E., McClusky, S., Reilinger, R. E., et al. (2002). Time–space variable afterslip on and deep below the Izmit earthquake rupture. *Bulletin of the Seismological Society of America*, *92*, 126–137.

Bürgmann, R., & Prescott, W. H. (2000). Monitoring the spatially and temporally complex active deformation field in the southern Bay area. *Final technical report. Collaborative research with University of California at Berkeley and U. S. Geological Survey, Menlo Park, CA, USA.*

Bürgmann, R., Rosen, P. A., & Fielding, E. J. (2000). Synthetic aperture radar interferometry to measure Earth's surface topography and its deformation. *Annual Review of Earth and Planetary Sciences*, *28*, 169–209.

Caltagirone, F., Angino, G., Impagnatiello, F., Capuzi, A., Fagioli, S., & Leonardi, R. (2007). COSMO-SkyMed: An Advanced Dual System for Earth Observation. *Proc. of the Int. Geosci. and Remote Sensing Symp. (IGARSS07), Barcelona*.

Cavalié, O., Lasserre, C., Doin, M. P., Peltzer, G., Sun, J., Xu, X., et al. (2008). Measurement of interseismic strain across the Haiyuan fault (Gansu, China), by InSAR. *Earth and Planetary Science Letters*, *275*, 246–257.

Chlieh, M., de Chabalier, J. B., Ruegg, J. C., Armijo, R., Dmowska, R., Campos, J., et al. (2004). Crustal deformation and fault slip during the seismic cycle in the North Chile subduction zone, from GPS and InSAR observations. *Geophysical Journal International*, *158*(2), 695–711.

Crosetto, M., Crippa, B., & Biescas, E. (2005). Early detection and in-depth analysis of deformation phenomena by radar interferometry. *Engineering Geology*, *79*(1–2), 81–91.

Dell'Acqua, F., Bignami, C., Chini, M., Lisini, G., Polli, D., & Stramondo, S. (2011). Earthquake rapid mapping by satellite remote sensing data: L'Aquila April 6th, 2009 event. *IEEE Journal of Selected Topics in Applied Earth Observations and Remote Sensing (JSTARS)*, *4*(4), 935–943, doi:10.1109/JSTARS.2011.2162721.

Deraw, D. (1999). Dinsar and coherence tracking applied to glaciology: the example of the Shirase Glacier. *ESA Fringe meeting 1999, Liège*.

Ergintav, S., Bürgmann, R., McClusky, S., Çakmak, R., Reilinger, R., Lenk, O., et al. (2002). Postseismic deformation near the Izmit earthquake (17 August 1999,M7.5) rupture zone. *Bulletin of the Seismological Society of America*, *92*, 194–207.

ESA (2010). The GMES Sentinels. http://www.esa.int/SPECIALS/Operations/SEM98Z8L6VE_0.html

Feigl, K., Sarti, F., Vadon, H., McClusky, S., Ergintav, S., Durand, P., et al. (2002). Estimating slip distribution for the Izmit mainshock from coseismic GPS, ERS-1, RADARSAT, and SPOT measurements. *Bulletin of the Seismological Society of America*, *92*(1), 138–160.

Ferretti, A., Fumagalli, A., Novali, F., Prati, C., Rocca, F., & Rucci, A. (2009). *The second generation PSInSAR approach: SqueeSAR, presented at the FRINGE2009 ESA Conference, Frascati, Italy*.

Ferretti, A., Prati, C., & Rocca, F. (2000). Nonlinear subsidence rate estimation using permanent scatterers in differential SAR interferometry. *IEEE Transactions on Geoscience and Remote Sensing*, *38*(5), 2202–2212.

Ferretti, A., Prati, C., & Rocca, F. (2001). Permanent scatterers in SAR interferometry. *IEEE Transactions on Geoscience and Remote Sensing*, *39*(1), 8–20.

Fialko, Y. (2004). Evidence of fluid-filled upper crust from observations of postseismic deformation due to the 1992 Mw7.3 Landers earthquake. *Journal of Geophysical Research*, *109*, B08401, doi:10.1029/2003JB002985.

Fialko, Y. (2006). Interseismic strain accumulation and the earthquake potential on the southern San Andreas fault system. *Nature*, *441*, 968–971.

Fielding, E. J., Lundgren, P. R., Bürgmann, R., & Funning, G. J. (2009). Shallow fault-zone dilatancy recovery after the 2003 Bam, Iran earthquake. *Nature*, *458*, 64–68.

Fielding, E. J., Talebian, M., Rosen, P. A., Nazari, H., Jackson, J. A., Ghorashi, M., et al. (2005). Surface ruptures and building damage of the 2003 Bam, Iran earthquake mapped by satellite synthetic aperture radar interferometric correlation. *Journal of Geophysical Research*, *110*, B03302, doi:10.1029/2004JB003299.

Fielding, E. J., Wright, T., Muller, J., Parsons, B., & Walker, R. (2004). Aseismic deformation of a fold-and-thrust belt imaged by synthetic aperture radar interferometry near Shahdad, southeast Iran. *Geology*, *32*, 577–580, doi:10.1130/G20452.1.

Funning, G. J., Barke, R. M. D., Lamb, S. H., Minaya, E., Parsons, B. E., & Wright, T. J. (2005). The 1998 Aiquile, Bolivia earthquake: An active fault revealed with InSAR,. *Earth and Planetary Science Letters*, *232*, 39–49.

Funning, G. J., Bürgmann, R., Ferretti, A., Novali, F., & Fumagalli, A. (2007). Creep on the Rodgers Creek Fault, northern San Francisco Bay area from a 10 year PS-InSAR dataset. *Geophysical Research Letters*, *34*(19), L19306.

Funning, G. J., Parsons, B., Wright, T. J., Jackson, J. A., & Fielding, E. J. (2005). Surface displacements and source parameters of the 2003 Bam, Iran earthquake from Envisat Advanced Synthetic Aperture Radar imagery. *Journal of Geophysical Research*, *110*(B9), B09406, doi:10.1029/2004JB003338.

Geller, R. J. (1997). Earthquake prediction: A critical review. *Geophysical Journal International*, *131*(3), 425–450.

Geller, J. R., Jackson, D. D., Kagan, Y. Y., & Mulargia, Y. F. (1996). Earthquakes cannot be predicted. *Science Online*, *275*(5306), 1616.

Gray, A. L., Mattar, K. E., Vachon, P. W., Bindschadler, R., Jezek, K. C., Forster, R., et al. (1998). InSAR results from the RADARSAT Antarctic Mapping Mission Data: Estimation of Glacier Motion using a simple Registration Procedure. *Proceedings of IGARSS'98, Seattle*.

Hearn, E. H., Bürgmann, R., & Reilinger, R. E. (2002). Dynamics of Izmit earthquake postseismic deformation and loading of the Düzce earthquake hypocenter. *Bulletin of the Seismological Society of America*, *92*, 172–193.

Hearn, E. H., Johnson, K., & Thatcher, W. (2010). Space Geodetic Data Improve Seismic Hazard Assessment in California. *Eos Transactions Agu*, *91*(38), doi:10.1029/2010EO380007.

Hobiger, T., Kinoshita, Y., Shimizu, S., Ichikawa, R., Furuya, M., Kondo, T., et al. (2010). On the importance of accurately ray-traced troposphere corrections for Interferometric SAR data. *Journal of Geodesy*, *84*(9), 537–546, doi:10.1007/s00190-010-0393-3.

Hooper, A. (2008). A multi-temporal InSAR method incorporating both persistent scatterer and small baseline approaches. *Geophysical Research Letters*, *35*, L16302, doi:10.1029/2008GL034654.

Hooper, A., Zebker, H., Segall, P., & Kampes, B. (2004). A new method for measuring deformation on volcanoes and other natural terrains using InSAR persistent scatterers. *Geophysical Research Letters*, *31*, L23611, doi:10.1029/2004GL021737.

Hsu, Y. -J., Simons, M., Avouac, J. -P., Galetzka, J., Sieh, K., Chlieh, M., et al. (2006). Frictional afterslip following the 2005 Nias-Simeulue earthquake, Sumatra. *Science*, *312*, 1921–1926.

Hunstad, I., Pepe, A., Atzori, S., Tolomei, C., Salvi, S., & Lanari, R. (2009). Surface deformation in the Abruzzi region, central Italy, from multitemporal DInSAR analysis. *Geophysical Journal International*, *178*(3), 1193–1197.

Hyndman, R. D., & Wang, K. (1993). Thermal constraints on the zone of major thrust earthquake failure: the Cascadia subduction zone. *Journal of Geophysical Research*, *98*, 2039–2060.

Jackson, J., Bouchon, M., Fielding, E., Funning, G., Ghorashi, M., Hatzfeld, D., et al. (2006). Seismotectonic, rupture process, and earthquake-hazard aspects of the 2003 December 26 Bam, Iran, earthquake. *Geophysical Journal International*, *166*(3), 1270–1292.

Jackson, D. D., Kagan, Y. Y., & Mulargia, F. (1997). Earthquakes cannot be predicted. *Science*, *275*, 1616.

Jacobs, A., Sandwell, D., Fialko, Y., & Sichoix, L. (2002). The 1999 Mw 7.1 Hector Mine, California, Earthquake: Near-Field Postseismic Deformation from ERS Interferometry. *Bulletin of the Seismological Society of America*, *92*(4), 1433–1442.

Jonsson, S., Segall, P., Pederson, R., & Bjornsson, G. (2003). Post-earthquake ground movements correlated to pore-pressure transients. *Nature*, *424*, 179–183.

Jónsson, S., Zebker, H., Segall, P., & Amelung, F. (2002). Fault slip distribution of the 1999 Mw7.2 Hector Mine Earthquake, California, estimated from satellite Radar

and GPS measurements. *Bulletin of the Seismological Society of America*, *92*(4), 1377–1389.
King, G. C. P., Stein, R. S., & Lin, J. (1994). Static stress changes and the triggering of earthquakes. *Bulletin of the Seismological Society of America*, *84*, 935–953.
Lanari, R., Mora, O., Manunta, M., Mallorquí, J. J., Berardino, P., & Sansosti, E. (2004). A small-baseline approach for investigating deformations on full-resolution differential SAR interferograms. *IEEE Transactions on Geoscience and Remote Sensing*, *42*(7), 1377–1386.
Lanari, R., et al. (2010). Surface displacements associated with the L'Aquila 2009 Mw 6.3 earthquake (central Italy): New evidence from SBAS-DInSAR time series analysis. *Geophysical Research Letters*, *37*, L20309, doi:10.1029/2010GL044780.
Lettieri, E., Masella, C., & Radaelli, G. (2009). Disaster management: Findings from a systematic review. *Disaster Prevention and Management*, *18*(2), 117–136.
Lohman, R. B., Simons, M., & Savage, B. (2002). Location and mechanism of the Little Skull Mountain earthquake as constrained by radar interferometry and seismic waveform modeling. *Journal of Geophysical Research*, *107*(B6), 2118, doi:10.1029/2001JB000627.
Lundgren, P., & Stramondo, S. (2002, November). Slip Distribution of the 1997 Umbria-Marche earthquake sequence through joint inversion of GPS and DInSAR data. *Journal of Geophysical Research*, *107*(B11), 2316, doi:10.1029/2000JB000103.
Lyons, S., & Sandwell, D. (2003). Fault creep along the southern San Andreas from interferometric synthetic permanent scatterers, and stacking. *Journal of Geophysical Research*, *108*(B1), 2047, doi:10.1029/2002JB001831.
Massonnet, D., Feigl, K., Rossi, M., & Adragna, F. (1994). Radar interferometric mapping of deformation in the year after the Landers earthquake. *Nature*, *369*, 227–230.
Massonnet, D., Feigl, K. L., Vadon, H., & Rossi, M. (1996). Coseismic deformation field of the M56.7 Northridge, California, earthquake of January 17, 1994, recorded by two radar satellites using nterferometry. *Geophysical Research Letters*, *23*(9), 969–972.
Massonnet, D., Rossi, M., Carmona, C., Adragna, F., Peltzer, G., Fiegl, K., et al. (1993). The displacement field of the Landers earthquake mapped by radar interferometry. *Nature*, *364*, 138–142.
Masterlark, T. (2003). Finite element model predictions of static deformation from dislocation sources in a subduction zone: Sensivities to homogeneous, isotropic, Poisson-solid, and half-space assumptions. *Journal of Geophysical Research*, *108*(B11), 2540, doi:10.1029/2002JB002296.
Matsuoka, M., & Yamazaki, F. (2001). Image processing of building damage detection due to disasters using SAR intensity images. *Proc. of 31st Conference of the Remote Sensing Society of Japan* (pp. 269–270)..
Matsuoka, M., & Yamazaki, F. (2002). Application of the Damage Detection Method Using SAR Intensity Images to Recent Earthquakes. *Proc. Int. Geoscience and Remote Sensing Symp., IGARSS 2002*.
Matsuoka, M., & Yamazaki, F. (2004). Building Damage Detection Using Satellite SAR Intensity Images for the 2003 Algeria and Iran Earthquake. *Proc. Int. Geoscience and Remote Sensing Symp., IGARSS 2004*.
McCloskey, J., & Nalbant, S. (2009). Near-real-time aftershock hazard maps. *Nature Geoscience*, *2*, 154–155, doi:10.1038/ngeo449.
Miyazaki, S., Segall, P., Fukuda, J., & Kato, T. (2004). Space time distributions of afterslip following the 2003 Tokachi-oki earthquake: Implications for variations in fault zone frictional properties. *Geophysical Research Letters*, *31*, doi:10.1029/2003GL019410.
Mora, O., Mallorquí, J. J., & Broquetas, A. (2003). Linear and nonlinear terrain deformation maps from a reduced set of interferometric SAR images. *IEEE on Transaction Geoscience and Remote Sensing*, *41*, 2243–2253.
Moro, M., Saroli, M., Salvi, S., Stramondo, S., & Doumaz, F. (2007). The relationship between seismic deformation and deep-seated gravitational movements during the 1997 Umbria-Marche (Central Italy) earthquakes. *Geomorphology*, *89*, 297–307.
Moro, M., Chini, M., Saroli, M., Atzori, S., Stramondo, S., & Salvi, S. (2011). Analysis of large, seismically induced, gravitational deformations imaged by high-resolution COSMO-SkyMed synthetic aperture radar. *Geology*, *39*(6), 527–530, doi:10.1130/G31748.1.
Motagh, M., Hoffmann, J., Kampes, B., Baes, M., & Zschau, J. (2007). Strain accumulation across the Gazikoy–Saros segment of the North Anatolian Fault inferred from Persistent Scatterer Interferometry. *Earth and Planetary Science Letters*, doi:10.1016/j.epsl.2007.01.003.
Nof, R. N., Baer, G., Eyal, Y., & Novali, F. (2008). Current surface displacement along the Carmel Fault system in Israel from the InSAR stacking and PSInSAR. *Israel Journal of Earth-Sciences*, *57*(2), 71–86.
Okada, Y. (1985). Surface deformation due to shear and tensile faults in a half-space. *Bulletin of the Seismological Society of America*, *75*, 1135–1154.
Parsons, T., & Dreger, D. S. (2000). Static-stress impact of the 1992 Landers earthquake sequence on nucleation and slip at the site of the 1999 M7.1 Hector Mine earthquake, southern California. *Geophysical Research Letters*, *27*, 1949–1952.
Peltzer, G., Crampe, F., Hensley, S., & Rosen, P. (2001). Transient strain accumulation and fault interaction in the Eastern California Shear Zone. *Geology*, *29*(11), 975–978.
Petersen, M., Cao, T., Campbell, K., & Frankel, A. (2007). Time-independent and time-dependent seismic hazard assessment for the state of California: uniform California earthquake rupture forecast model 1.0. *Seismological Research Letters*, *78*(1), 99–109.
Pollitz, F. (2005). Transient rheology of the upper mantle beneath central Alaska inferred from the crustal velocity field following the 2002 Denali earthquake. *Journal of Geophysical Research*, *110*, B08407.
Pollitz, F., Peltzer, G., & Bürgmann, R. (2000). Mobility of continental mantle: Evidence from postseismic geodetic observations following the 1992 Landers earthquake. *Journal of Geophysical Research*, *105*, 8035–8054.
Pollitz, F., Wicks, C., & Thatcher, R. (2001). Mantle flow beneath a continental strike-slip fault: postseismic deformation after the 1999 Hector Mine earthquake. *Science*, *293*, 1814–1818.
Prati, C., Ferretti, A., & Perissin, D. (2010). Recent advances on surface ground deformation measurement by means of repeated space-borne SAR observations. *Journal of Geodynamics*, *49*(3–4), 161–170.
Pritchard, M. E., Ji, C., & Simons, M. (2006). Distribution of slip from 11Mw > 6 earthquakes in the northern Chile subduction zone. *Journal of Geophysical Research*, *111*, doi:10.1029/2005JB004013.
Rundle, J. B., Turcotte, D. L., Shcherbakov, R., Klein, W., & Sammis, C. (2003). Statistical physics approach to understanding the multiscale dynamics of earthquake fault systems. *Reviews of Geophysics*, *41*, 1019.
Ryder, I., Parsons, B., Wright, T. J., & Funning, G. J. (2007). Postseismic motion following the 1997 Manyi (Tibet) earthquake: InSAR observations and modelling. *Geophysical Journal International*, *169*, 1009–1027.
Sakamoto, M., Takasago, Y., Uto, K., Kakumoto, S., & Kosugi, Y. (2004). Automatic Detection of Damaged Area of Iran Earthquake by High-Resolution Satellite Imagery. *Proc. Geoscience and Remote Sensing Symp., IGARSS 2004*.
Salvi, S., Stramondo, S., Cocco, M., Tesauro, M., Hunstad, I., Anzidei, M., et al. (2000). Modeling coseismic displacements resulting from SAR Interferometry and GPS measurements during the 1997 Umbria-Marche seismic sequence. *Journal of Seismology*, *4*(4), 479–499.
Salvi, S., Vignoli, S., Serra, M., & Bosi, V. (2009). Use of Cosmo-Skymed data for seismic risk management in the framework of the ASI-SIGRIS project. *Proc. Geoscience and Remote Sensing Symp., IGARSS 2009* (pp. II–921 – II-924)., doi: 10.1109/IGARSS.2009.5418248.
Salvi, S., Vignoli, S., Zoffoli, S., & Bosi, V. (2010). Use of satellite SAR data for seismic risk management: results from the pre-operational ASI-SIGRIS project. *Proc. ESA Living Planet Symposium, European Space Agency Special Publication SP-686*.
Sandwell, D., Sichoix, L., Agnew, D., Bock, Y., & Minster, J. -B. (2000). Near real-time radar interferometry of the Mw 7.1 Hector Mine Earthquake. *Geophysical Research Letters*, *27*, 3101–3104.
Sansosti, E., Casu, F., Manzo, M., & Lanari, R. (2010). Space-borne radar interferometry techniques for the generation of deformation time series: An advanced tool for Earth's surface displacement analysis. *Geophysical Research Letters*, *37*, L20305, doi:10.1029/2010GL044379.
Sarti, F., Briole, P., & Pirri, M. (2006). Coseismic fault rupture detection and slip measurement by ASAR precise correlation using coherence maximization: application to a north–south Blind Fault in the Vicinity of Bam (Iran). *IEEE Geoscience and Remote Sensing Letters*, *3*(2), 187–191.
Savage, J. C., & Burford, R. O. (1973). Geodetic determination of relative plate motion in central California. *Journal of Geophysical Research*, *78*, 832–845, doi: 10.1029/JB078i005p00832.
Schmidt, D. A., Bürgmann, R., Nadeau, R. M., & d'Alessio, M. (2005). Distribution of aseismic slip rate on the Hayward fault inferred from seismic and geodetic data. *Journal of Geophysical Research*, *110*, B08406, doi:10.1029/2004JB003397.
Simons, M., Fialko, Y., & Rivera, L. (2002). Coseismic deformation from the 1999 Mw 7.1 Hector Mine, California earthquake as inferred from InSAR and GPS observations. *Bulletin of the Seismological Society of America*, *92*, 1390–1402.
Snoeij, P., Attema, E., Duesmann, B., Rommen, B., Floury, N., Davidson, M., et al. (2010). Sentinel-1 Coverage and Revisit Capabilities. *Proc. ESA Living Planet Symposium, European Space Agency Special Publication SP-686*.
Steacy, S., Gomberg, J., & Cocco, M. (2005). Introduction to special section: Stress dependent seismic hazard. *Journal of Geophysical Research*, *110*, B05S01, doi: 10.1029/2005JB003692.
Stein, R. S. (1999). The role of stress transfer in earthquake occurrence. *Nature*, *402*, 605–609.
Stramondo, S., Bignami, C., Chini, M., Pierdicca, N., & Tertulliani, A. (2006). The radar and optical remote sensing for damage detection: Results from different case studies. *International Journal of Remote Sensing*, *27*, 20.
Stramondo, S., Tesauro, M., Briole, P., Sansosti, E., Salvi, S., Lanari, R., et al. (1999). The September 26, 1997 Colfiorito, Italy, earthquakes: Modeled coseismic surface displacement from SAR interferometry and GPS. *Geophysical Research Letters*, *26*(7), 883–886.
Taylor, M. H., & Peltzer, G. (2006). Current slip rates on conjugate strike slip faults in Central Tibet using Synthetic Aperture Radar Interferometry. *Journal of Geophysical Research*, *B12402*, doi:10.1029/2005JB004014.
Usai, S. (2003). A least squares database approach for SAR interferometric data. *IEEE Transactions on Geoscience and Remote Sensing*, *41*(4), 753–760.
Werner, C., Wegmuller, U., Strozzi, T., & Wiesmann, A. (2003). *Interferometric point target analysis for deformation mapping. Proceedings of IGARSS '03*, *vol. 7*. (pp. 4362–4364).
Werninghaus, R. (2006). The TerraSAR-X Mission. *Proc. 6th European Conference on Synthetic Aperture Radar, Dresden, Germany*.
Weston, J., Ferreira, A. M., & Funning, G. J. (2011). Global compilation of InSAR earthquake source models: 1. Comparison with seismic catalogs. *Journal of Geophysical Research*, *116*, B08408, doi:10.1029/2010JB008131.
Wright, T. J., Lu, Z., & Wicks, C. (2003). Source model for the M-w 6.7, 23 October 2002, Nenana Mountain Earthquake (Alaska) from InSAR. *Geophysical Research Letters*, *30*, doi:10.1029/2003GL018014.
Wright, T., Lu, Z., & Wicks, C. (2004). Constraining the slip distribution and fault geometry of the Mw7.9, 2 November 2002, Denali Fault Earthquake with interferometric synthetic aperture radar and global positioning system data. *Bulletin of the Seismological Society of America*, *94*(6B), S175–S189.
Wright, T. J., Parsons, B., England, P. C., & Fielding, E. J. (2004). InSAR observations of low slip rates on the major faults of western Tibet. *Science*, *305*, 236–239.
Wright, T. J., Parsons, B., & Fielding, E. (2001). Measurement of interseismic strain accumulation across the North Anatolian Fault by satellite radar interferometry. *Geophysical Research Letters*, *28*, 2117–2120.
Wright, T. J., Parsons, B. E., Jackson, J. A., Haynes, M., Fielding, E. J., England, P. C., et al. (1999). Source parameters of the 1 October 1995 Dinar (Turkey) earthquake from SAR interferometry and seismic bodywave modelling. *Earth and Planetary Science Letters*, *172*, 23–37.

Wright, T. J., Parsons, B. E., & Lu, Z. (2004). Toward mapping surface deformation in three dimensions using InSAR. *Geophysical Research Letters*, *31*, doi:10.1029/2003GL018827.

Xinjian, S., & Guohong, Z. (2007). A characteristic analysis of the dynamic evolution of preseismic-coseismic-postseismic interferometric deformation fields associated with the M7.9 Earthquake of Mani, Tibet in 1997. *Acta Geologica Sinica (English Edition)*, *81*(4), 587–592.

Yin, Y. P., Wang, F. W., & Sun, P. (2009). Landslide hazards triggered by the 2008 Wenchuan earthquake, Sichuan, China. *Landslides*, *6*, 139–152.

Yonezawa, C., & Takeuchi, S. (2001). Decorrelation of SAR data by urban damages caused by the 1995 Hoyogoken-nanbu earthquake. *International Journal of Remote Sensing*, *22*(8), 1585–1600.

Zebker, H., Rosen, P., & Hensley, S. (1997). Atmospheric effects in interferometric synthetic aperture radar surface deformation and topographic maps. *Journal of Geophysical Research*, *102*, 7547–7563.

Zebker, H., & Villasenor, J. (1992). Decorrelation in interferometric radar echoes. *IEEE Transactions on Geoscience and Remote Sensing*, *30*, 950–959.